Journal of Inflammation Research

Dovepress
Taylor & Francis Group

Open Access Full Text Article

ORIGINAL RESEARCH

The Role of EZH2 in Initiating Epigenetic Regulation of CRSwNP

Rong Zeng[1,*], Yakun Wang[2,*], Xinyu Song[1,*], Jianting Wang[1]

[1]Department of Otorhinolaryngology, Head and Neck Surgery, Beijing Chaoyang Hospital, Capital Medical University, Beijing, 100020, People's Republic of China; [2]Department of Dermatology, Venereology and Cosmetology, Beijing Chaoyang Hospital, Capital Medical University, Beijing, 100020, People's Republic of China

*These authors contributed equally to this work

Correspondence: Jianting Wang, Department of Otorhinolaryngology, Head and Neck Surgery, Beijing Chaoyang Hospital, Capital Medical University, Beijing, 100020, People's Republic of China, Email tingjw@126.com

Purpose: Chronic rhinosinusitis with nasal polyps (CRSwNP) was a polygenic disease whose pathogenesis involved epigenetic mechanisms. This study aimed to analyze biomarkers and pathways associated with CRSwNP using RNA-sequencing and explore the role of key biomarkers in the inflammatory response through epigenetic regulation in nasal mucosal cells. Particularly on EZH2, a key epigenetic regulator and histone methyltransferase, to explore its potential for CRSwNP immunotherapy.

Patients and Methods: A total of 86 individuals were included between July 2021 and July 2023, including 43 patients with CRSwNP who underwent nasal polyp surgery and 43 patients with a deviated septum. Initially, differentially expressed genes (DEGs) between CRSwNP and control groups were screened using the obtained transcriptomic sequencing CRSwNP dataset. Biomarkers were filtered using machine learning algorithms and validated using immunohistochemistry (IHC) and quantitative real-time reverse transcription polymerase chain reaction (qRT-PCR). The expression of enhancer of zeste homolog 2 (EZH2) was knocked down via siRNA and overexpressed through plasmid transfection in human nasal epithelial cells (HNEpCs). The effects of EZH2 overexpression and knockdown on the expression of high-mobility gene group A2 (HMGA2) activation and H3k27me3 expression were assessed using qRT-PCR and immunofluorescence.

Results: EZH2, insulin-like growth factor 2 mRNA-binding protein 1 (IGF2BP1), and HMGA2 were revealed as potential biomarkers which screened from five target genes. Gene set enrichment analysis and immune infiltration analysis revealed the most critical gene was EZH2, with its expression exhibiting a positive relationship with HMGA2. Moreover, EZH2 knockdown upregulated H3k27me3 expression and inhibited HMGA2 activation. In contrast, EZH2 overexpression downregulated H3k27me3 expression and promoted HMGA2 activation. Notably, the expression levels of IGF2BP1, EZH2, and HMGA2 were higher in the CRSwNP group than in the control group.

Conclusion: This study identified three potential biomarkers, IGF2BP1, EZH2, and HMGA2, associated with CRSwNP. Notably, EZH2 could serve as a new adjuvant immunotherapy target in CRSwNP through the modulation of epigenetic mechanisms.

Keywords: CRSwNP, whole transcriptome sequencing, EZH2, epigenetic regulation, immunotherapy

Introduction

Chronic rhinosinusitis (CRS) is an inflammatory process affecting the mucosa of the nasal cavity and one or more sinuses. Its clinical manifestations include nasal congestion, nasal leakage, loss or reduction of the sense of smell, and facial or head pain, lasting for more than 12 weeks. These symptoms severely affect the quality of life of patients and impose substantial social and economic burdens.[1] The pathogenesis of CRS is complex, involving genetic factors, the sinus microbiota, infections, and environmental influences, and has not yet been fully elucidated.[2] Clinically, CRS is generally classified into two subtypes: CRS without nasal polyps (CRSsNP) and CRS with nasal polyps (CRSwNP), with a prevalence ratio of approximately 4:1. This disease is also characterized by its pathophysiological mechanisms. These mechanisms are further classified into type 2 inflammation and non-type 2 inflammation based on the characteristics of

Received: 29 March 2025
Accepted: 19 June 2025
Published: 1 July 2025

the main effector T cells and innate lymphoid cells (ILCs) involved in the inflammatory response.[3,4] These distinct inflammatory endotypes reflect the involvement of different immune cell types (eg, T cells, B cells) and cytokines in the immune system.[5,6] In diseases such as CRSwNP, variations in inflammatory endotypes may influence disease progression, symptom severity, and treatment responsiveness. The primary pharmacological treatments for CRSwNP include topical and oral glucocorticosteroids, antibiotics, antihistamines, antileukotrienes, and saline nasal rinses. However, conventional therapies often overlook the phenotypic differences and intrinsic pathophysiological mechanisms of CRSwNP, resulting in limited symptomatic relief.[7] Currently, the disease is incurable and prone to frequent recurrence. Multiple clinical and biomarker parameters have been reported to be associated with type 2 inflammation and response to biologic therapies, including clinical scores (eg, SNOT-22, LMS) and nasal secretion markers (eg, eosinophil cationic protein, interleukin-5, etc). However, approximately 40–60% of patients show poor response to these biologics, and the predictive validity of these biomarkers still requires further verification.[8] Additionally, the complexity of gene expression patterns in CRSwNP represents a crucial factor in fully understanding its underlying pathogenesis. Therefore, the development of clinically applicable biomarkers would enable personalized treatment approaches for CRSwNP patients and could potentially significantly improve therapeutic outcomes.

Whole transcriptome RNA-sequencing (RNA-seq) is a robust technique used to analyze the complete genome of RNA extracted from tissues.[9] By comparing the transcriptome of nasal polyps with that of control nasal mucosa, gene mutations associated with the disease can be identified. Moreover, this approach can reveal molecular differences between different types of CRSwNP, which may serve as potential therapeutic targets, thus contributing to the development of personalized treatment options.[10] Therefore, RNA-seq serves as a powerful tool for identifying gene signatures and candidate pathways associated with the pathogenesis of CRSwNP, informing novel potential therapeutic targets.

Currently, the recommended treatment for CRSwNP includes pharmacological therapy with systemic (oral) and topical (nasal) glucocorticoids, antimicrobial agents, antihistamines, and leukotriene receptor antagonists.[11] However, some patients with severe disease do not respond adequately to pharmacological therapies and may require repeated systemic corticosteroid courses and/or sinus surgery.[12] Even after successful surgery, recurrence rate can still be as high as 40% within 18 months, with approximately 80% of patients experiencing recurrence after 12 years. The occurrence of some inflammatory diseases (such as autoimmune diseases, allergic diseases, etc) is related to epigenetic changes.[13,14] Epigenetic regulation refers to the modulation of cellular behavior through alterations in gene expression patterns without changing the DNA sequence, typically involved in processes such as cell differentiation, development, and stress responses.[15] In these diseases, the epigenetic regulation of genes is abnormal, leading to the overproduction of inflammatory factors and the persistence of the inflammatory response. Inflammatory factors (such as tumor necrosis factor-α, interleukin-1, interleukin-6, etc) regulate histone modification, DNA methylation, and non-coding RNA expression, thereby affecting gene expression and cell function. The inflammatory microenvironment affects the epigenetic characteristics of stem cells, causing them to differentiate into inflammatory cells or fibrocytes.[16] In addition, inflammatory factors and inflammatory cells can also regulate the proliferation, invasion and metastasis of tumor cells by influencing the epigenetic characteristics of tumor cells.[17] In conclusion, there is a strong link between inflammation and epigenetics. Signaling molecules produced during inflammation can affect epigenetic regulatory mechanisms, and epigenetic changes can also affect the occurrence and development of inflammatory responses. This interaction is of great significance for the occurrence and development of inflammation-related diseases, and also provides new ideas for the treatment of inflammation-related diseases. In recent years, biologic agents targeting type 2 inflammation have emerged as a potential avenue for individualized treatment in difficult-to-control, severe CRSwNP cases.[18] Furthermore, although plasma IgE levels are also increased in patients with CRSwNP, there is no association of these IgE levels with the presence of atopy or environmental allergies. It is not yet clear what clinical benefit may be seen if CRSwNP patients are treated with an anti-IgE agent.[19] Previous studies have used RNA sequencing to identify transcriptome signature, gene features and candidate pathways associated with CRSwNP by comparing CRSwNP patients and controls will help identify disease targets. The known biological processes implicated in CRSwNP are multifaceted, including airway inflammation, tight junction impairment, pathogen infection and a defective host defence.[20] Although eosinophilia reportedly predisposes NP formation.[21] Interestingly, in the study by yang et al, suggested that eosinophilia was not

a major confounder. The unique DEGs for the aforementioned comparisons revealed that pathways associated with the molecular mechanisms of cancer and neutrophil N-formylmethionyl-leucyl-phenylalanine signaling drive polyp formation. Suppressing exaggerated cell growth might, therefore, be an effective management approach for CRSwNP in the future, given that the rapid recurrence of CRSwNP mimics benign tumor growth.[22] These biologics primarily act through several mechanisms, including anti-IgE, anti-interleukin (IL)-4Ra, anti-IL-5, and anti-IL-5Ra, blocking specific inflammatory factors or receptors to modulate the inflammatory response.[23] However, the complete remission rate with immunotherapy alone for CRSwNP remains low. Notably, increasing evidence suggests that epigenetic dysregulation is a key factor in the poor response to chemoimmunotherapy in patients with CRSwNP.[15] Epigenetics regulates gene expression through DNA methylation, histone modification, and non-coding RNA editing.[24] Among them, DNA methylation is integral to gene expression and plays an important role in inflammation. Therefore, normalizing epigenetic regulation is essential to improving the success of immunotherapy for CRSwNP.[25]

Enhancer of zeste homolog 2 (EZH2) is the catalytic subunit of the polycomb repressive complex 2 (PRC2). It inhibits the transcription of its target genes by catalyzing the trimethylation of lysine 27 on histone H3 (H3K27me3).[26] EZH2 plays a crucial role in regulating the division of various immune cells in allergic rhinitis. For example, the exosomal long non-coding RNA GAS5 inhibits Th1 differentiation and promotes Th2 differentiation by downregulating the expression of both EZH2 and T-bet.[27] EZH2 deficiency in CD4+ T cells enhances the Th2 immune response in ovalbumin (OVA)-induced allergic airway models.[28] Moreover, 3-deazaneplanocin A, an indirect inhibitor of EZH2, inhibits dendritic cell activation in vitro.[29] Therefore, EZH2, as a central regulator of immune cell differentiation in allergic rhinitis, plays an important role in chronic inflammation.

In the present study, we aimed to identify biomarkers and pathways associated with the pathogenesis of CRSwNP. To this end, we performed RNA-seq in polyp tissues and normal mucosal tissues to identify transcriptomic features associated with CRSwNP. We also conducted a comprehensive analytical pipeline to determine differentially expressed genes (DEGs) and gene sets enriched in functional pathways. Moreover, we investigated the involvement of key biomarkers in the inflammatory response of CRSwNP through epigenetic regulation in nasal mucosal epithelial cells. This study offers new research directions for the application of immunotherapy in CRSwNP.

Materials and Methods

Source of Data

This work was approved by the Institutional Review Board (2022-department-564) of the Ethics Committee of Beijing Chaoyang Hospital. All human studies were conducted according to institutional ethical norms and the guidelines outlined in the Declaration of Helsinki. All participants provided written informed consent before participation. A total of 86 individuals were included between July 2021 and July 2023, comprising 43 patients with CRSwNP who underwent nasal polyp surgery and another 43 patients who had a deviated septum surgically corrected. CRSwNP was diagnosed following the European Position Paper on Rhinosinusitis and Nasal Polyps 2020 guidelines.[30] Patients who had taken oral glucocorticoids, antimicrobials, anti-leukotrienes, or antihistamines within four weeks prior to sample collection were excluded from the study. Moreover, patients with concurrent aspirin sensitivity, allergic rhinitis, or asthma, along with a deviated nasal septum, were also excluded. The control group consisted of 43 patients with septal deviation, while the CRSwNP group comprised 43 patients with CRSwNP. Eight pairs of samples (8 chronic rhinosinusitis with nasal polyps and 8 control samples) were collected for transcriptome sequencing to generate the CRSwNP transcriptome sequencing (TS-CRSwNP) dataset. Immunohistochemistry (IHC) analysis was performed on tissue samples obtained from 20 patients with nasal polyps (NPs) in the CRSwNP group and 20 nasal mucosal tissue samples from the control group. Quantitative real-time reverse transcription polymerase chain reaction (qRT-PCR) analysis was performed using tissue samples from 15 patients with NP in the CRSwNP group and 15 nasal mucosal tissue samples from the control group for validation. The GSE136825 dataset, sourced from the Gene Expression Omnibus (GEO) database, was used for gene validation. This dataset (GPL20301) includes RNA-seq data from turbinate samples, including 42 CRSwNP samples, 33 nonpolyp inferior turbinate (CRSwNP-IT) samples and 28 control samples.[22] The flowchart of this study is shown in Figure 1.

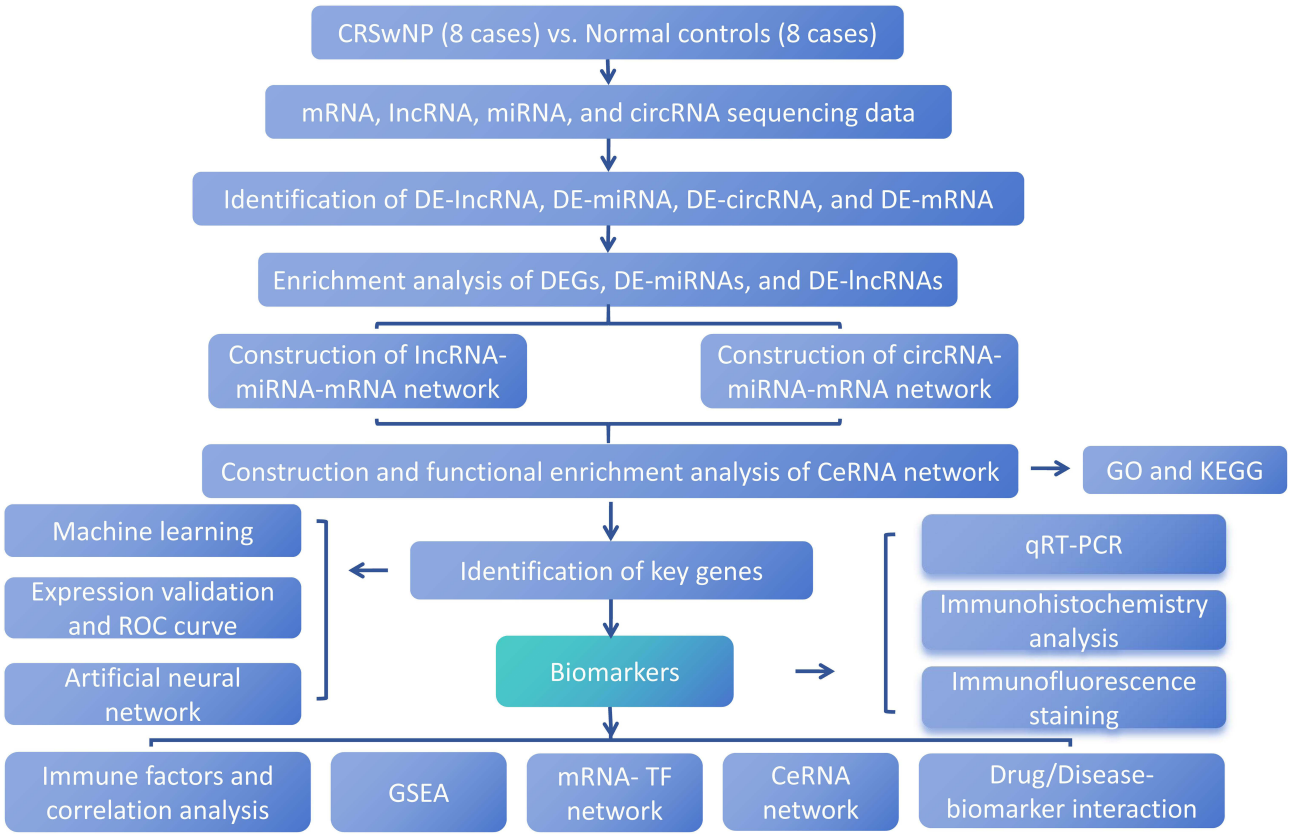

Figure 1 The flowchart of this study.

Transcriptomic Sequencing

Total RNA from nasal polyp samples was isolated using TRIzol (Invitrogen, Carlsbad, CA, USA) reagent, according to the manufacturer's instructions. The RNA concentration and purity were quantified using the NanoDrop ND-1000 spectrophotometer (NanoDrop, Wilmington, DE, USA). RNA integrity was evaluated through agarose gel electrophoresis. Oligo (dT) magnetic beads (Dynabeads Oligo [dT]; Thermo Fisher Scientific, Waltham, MA, USA) were used for the specific capture of mRNA with PolyA tails. Subsequently, fragmented RNA was reverse-transcribed into cDNA using SuperScript™ II Reverse Transcriptase (Invitrogen). Two-strand synthesis was performed using *Escherichia coli* DNA polymerase I (New England Biolabs [NEB], Ipswich, MA, USA) with RNase H (NEB, USA). The RNA-DNA hybrids were converted into double-stranded DNA. The second strand was digested using the UDG enzyme (NEB). PCR amplification was performed to construct a library with a fragment size of 300 ± 50bp. Finally, double-end sequencing was conducted using Illumina novaseq 6000 (LC Bio Technology CO., Ltd. Hangzhou, China) according to standard protocols.

Identification of DEGs, Differentially Expressed microRNAs (DE-miRNAs), Differentially Expressed-Long Non-Coding RNAs (DE-lncRNAs), and Differentially Expressed-Circular RNAs (DE-circRNAs)

DEGs, DE-miRNAs, DE-lncRNAs, and DE-circRNAs between the CRSwNP and control groups were identified using the DESeq2 package (v 1.38.0)[31] in the TS-CRSwNP dataset, applying the criteria of adjusted p value < 0.05 and $|\log_2 FC| > 0.5$.[32,33] The Benjamini - Hochberg (BH) method was used for calibration. Analysis of variance was visualized using a volcano map and a heatmap generated using the ggplot2 package (v 3.4.1)[34] and pheatmap package (v 1.0.12), respectively. The results for DE-circRNAs were displayed only via a volcano plot.

Functional Annotation of DEGs, DE-miRNAs, and DE-lncRNAs

The target mRNAs of DE-miRNA were predicted using miRTarBase and TarBase, and the DE-miRNA target genes were identified by intersecting the target mRNA and DE-mRNA after removing duplicates. The pairs of DE-lncRNAs and DE-mRNAs with a correlation coefficient (r) > 0.5 and $p < 0.05$ were screened using the Spearman method, and DE-lncRNAs target genes were obtained after removing duplicates. Gene Ontology (GO) and Kyoto Encyclopedia of Genes and Genomes (KEGG) enrichment analysis of DEGs, DE-miRNAs target genes, and DE-lncRNAs target genes were performed using the clusterProfiler package (v 4.7.1)[35] and org.Hs.eg.db (v 3.16.0) (p value < 0.05).

Construction of a Competing Endogenous RNAs (ceRNAs) Regulatory Network

The StarBase and miRNet databases were utilized to predict lncRNAs targeting miRNAs. The predicted lncRNAs were intersected with DE-lncRNAs to obtain co-lncRNAs. Combined with the prediction results from the previous step, the lncRNA-miRNA-mRNA network was constructed using Cytoscape software.[36]

The StarBase and circBank databases were utilized to predict circRNAs targeting miRNAs. The relationship pairs between circRNAs and DEGs with $r > 0.5$ and $p < 0.05$ were identified using the Spearman method. Finally, a circRNA-miRNA-mRNA network was constructed.

Integration of ceRNA Networks and Functional Enrichment

The lncRNA-miRNA-mRNA and circRNA-miRNA-mRNA networks were integrated, and relationships linked by the same miRNA were used to construct ceRNA networks. Genes within the ceRNA network were considered candidate genes. GO and the KEGG enrichment analysis of these candidate genes were performed using the clusterProfiler package (v 4.7.1)[35] and org.Hs.eg.db (v 3.16.0), with a significance threshold of $p < 0.05$.

Machine Learning Screening for Biomarkers

First, to explore the interactions between candidate genes, a protein–protein interaction (PPI) network was established using the STRING website (https://string-db.org) (confidence = 0.4). Subsequently, the sub-networks were analyzed using the plugin CytoHubba, which is capable of assigning values to each node in the network by applying multiple topological algorithms to identify key genes and sub-networks. Based on this, the five gene networks with the highest degree values were selected as the core networks, and the genes in the networks were identified as hub genes. Feature genes were first screened based on the hub genes using the XGBoost model, which was constructed via the xgboost package (v 1.7.3.1) (https://CRAN.R-project.org/package=xgboost). XGBoost is an ensemble learning algorithm based on gradient boosting decision trees, which can optimize model performance by adjusting various hyperparameters. In constructing the XGBoost model, max_depth was set to 5, eta to 0.3, objective to "binary:logistic", and nround to 25. Additionally, feature genes were screened using the Support Vector Machines-Recursive Feature Elimination (SVM-RFE) model, constructed using the caret package (v 6.0–93) (https://CRAN.R-project.org/package=caret). SVM-RFE identified the most critical feature subset for classification by progressively eliminating features. A five-fold cross-validation strategy was employed to more robustly evaluate model performance. Biomarkers were selected by overlapping SVM-RFE-feature-genes and XGBoost-feature-genes, and their diagnostic performance was assessed using receiver operating characteristic (ROC) curves. Finally, the correlation between the biomarkers was calculated using Spearman correlation analysis using the corrplot package (v 0.92) (https://github.com/taiyun/corrplot).

Construction of the Artificial Neural Network (ANN) Model

The ANN model was developed using a neural network software package based on biomarkers that minimizes the error between the model's predicted and actual values by adjusting the weights and biases.[37] The importance of each biomarker for the predictive outcome of the model was computed using the ANN network. Subsequently, the performance of the model was evaluated using a confusion matrix and ROC curve analysis.

Single-Gene Gene Set Enrichment Analysis (GSEA) Analysis

Single-gene GSEA was performed to identify the enriched regulatory pathways and biological functions of the biomarkers using clusterProfiler (v 4.7.1),[35] with adjusted $p < 0.05$ and normalized enrichment score $|NES| \geq 1$. The

results for the top 5 pathways with the largest absolute values of NES, both greater than 0 and less than 0, were visualized.

Relationship Between Biomarkers and Immune Factors

The CIBERSORT algorithm, which is specifically designed to estimate the abundance of different cell types in mixed cell populations, was used in this study to calculate the proportions of 15 immune cell subtypes in each sample (excluding immune cells with zero abundance in more than 75% of the samples).[38] To investigate the association between biomarkers and different immune features, the immune features (chemokines and major histocompatibility complex [MHC]) associated with CRSwNP were retrieved from the TISIDB database. Differential profiles of these immune features between the CRSwNP and control groups were then assessed using the Wilcoxon test. Finally, the correlation between biomarkers with differential immune cells, chemokines, and MHC was analyzed using the Spearman method.

Construction of a mRNA-Transcription Factor (TF) Network

To understand the transcriptional regulatory mechanisms of biomarkers, TFs targeting the biomarkers were predicted using the ChEA3 and NetworkAnalyst databases, and the mRNA-TF regulatory network was obtained using Cytoscape.[36]

Construction of Biomarker-Drug Interaction Network

To explore new therapeutic targets for CRSwNP treatment, drug predictions for biomarkers were performed. Initially, the DGIDB database (https://dgidb.org/) was used to predict potential drugs targeting the biomarkers. Subsequently, a biomarker-drug network was constructed based on the predicted results.

Analysis of Molecular Regulatory Axes

The sub-network containing biomarkers was extracted from the ceRNA network and displayed using the Sankey diagram.

Relationship Between Biomarkers and Diseases

To analyze the role of biomarkers in other ear-nose-throat (ENT) diseases, the Comparative Toxicogenomics (CTD) database (https://ctdbase.org/) was used to assess their association with various ENT conditions. The results are presented using bar charts.

Expression Analysis

To validate the expression of the biomarkers in CRSwNP and control tissues, expression analysis was performed using both the TS-CRSwNP and GSE136825 datasets.

Cell Lines and Culture

Human normal nasal mucosal epithelial cell line (HNEpCs) was obtained from WHELAB (Shanghai, China). Cells were cultured in epithelial cell media (M1005A; WHELAB) at 37°C in a 5% CO_2 incubator.

siRNA and Plasmid Transfection

The siRNA used in this study was developed by SyngenTech (Beijing, China). The plasmid for overexpression of EZH2 was synthesized by Thermo Fisher Scientific. Lipofectamine 3000 (Life Technologies, Thermo Fisher Scientific) was used for siRNA and plasmid transfections into HNEpCs, following the manufacturer's instructions. The siRNA sequences are as follows:siEZH2-1:5′-GACUCUGAAUGCAGUUGCUTT-3′;

siEZH2-2:5′-CGGCUCCUCUAACCAUGUUTT-3′; siEZH2-3:5′-CAGAAGAACUAAAGGAAAATT-3′; and control:5′-UUCUCCGAACGUGUCACGUTT-3′.

The sequence information on *EZH2* overexpression plasmids is available in the Supplementary Information 1. The empty vector pCDNA3_Zsgreen-T2A-puro was used as a control.

RNA Extraction, Reverse Transcription, and Quantitative Real-Time Reverse Transcription Polymerase Chain Reaction (qRT-PCR)

qRT-PCR is a technique used to measure the quantity of RNA in biological samples by converting RNA into DNA (cDNA) through reverse transcription and then amplifying and quantifying the cDNA in real-time using fluorescent markers. The First-Strand cDNA Synthesis Kit (Transgene, Beijing, China) was used to reverse-transcribe 1 g of the extracted total RNA. The resulting cDNAs were then assessed using the QuantStudioTM 5 System for qRT-PCR with SYBR mix (Transgene, Beijing, China).

The following primers were used:

EZH2: F, 5′-AATCAGAGTACATGCGACTGAGA-3′;

R,5′-GCTGTATCCTTCGCTGTTTCC-3′;

Insulin-like growth factor 2 mRNA-binding protein 1 (IGF2BP1): F, 5′-TCGTTGCAAGACCTTACCCTT-3′;

R, 5′-GGCAGCCACATCATTCTCATAG-3′;

High-mobility gene group A2 (HMGA2): F, 5′-CTCAAAAGAAAGCAGAAGCCACTG-3′;

R, 5′-TGAGCAGGCTTCTTCCGAACAACT-3′

GAPDH: F, 5′-GGAAGCTTGTCATCAATGGAAATC-3′;

R, 5′-TGATGACCCTTTTGGCTCCC-3′.

Immunohistochemistry (IHC) Analysis

Immunohistochemistry (IHC) analysis is a staining technique that utilizes the specificity of antibodies to target and visualize antigens in tissue sections, aiding in the understanding of cell types and their functions within a tissue. Tissue samples were heated at 65 °C for 2 h, then rehydrated and dewaxed using xylene and gradient ethanol. Samples were then boiled in an EDTA solution (pH = 8.0) for 20 min for antigen retrieval. To block non-specific binding, 2% goat serum was used. Tissue samples were then incubated with primary antibodies overnight at 4°C (anti-IGF2BP1, dilution 1:200; anti-EZH2, dilution 1:100; anti-HMGA2, dilution 1:100; all obtained from Abcam, Cambridge, UK).

Immunofluorescence (IF) Staining

IF staining is a technique used to visualize specific antigens in cells or tissues by labeling them with fluorescent antibodies, allowing for the detection and localization of these antigens under a microscope. The expression of H3k27me3 and HMGA2 was detected using immunofluorescence staining. Following a 20-min exposure to 4% paraformaldehyde, cells were blocked for 2 h at room temperature using 1% BSA (Gibco; Thermo Fisher Scientific) and 0.1% Triton-X. After overnight incubation at 4°C with the primary antibody against H3k27me3 (anti-H3k27me3, 1:1000 dilution; Cell Signaling Technology, Danvers, MA, USA) and HMGA2 (anti-HMGA2, 1:100 dilution; Abcam), the cells were incubated for 2 h at room temperature with the goat anti-rabbit IgG-H&L secondary antibody (cat. no. ab150077; 1:500; Abcam). Nuclei were stained with DAPI (Beyotime Institute of Biotechnology, Suzhou, China) for 5 min at room temperature, and stained cells were examined under a fluorescence microscope.

Statistical Analysis

All bioinformatics analyses were performed using R software (v 4.2.2) (R Foundation, Vienna, Austria). The Benjamini - Hochberg method was used for calibration. Spearman correlation analysis was conducted to assess relationships between variables. Data from different groups were compared using the Wilcoxon test, with $p < 0.05$ considered statistically significant.

Results

Acquisition of DEGs, DE-miRNAs, and DE-lncRNAs and Construction of lncRNA-miRNA-mRNA and CircRNA-miRNA-mRNA Networks

In total, 3298 DEGs (2683 upregulated and 615 downregulated), 201 DE-miRNAs (105 upregulated and 96 downregulated), 204 DE-lncRNAs (170 upregulated and 34 downregulated), and 16 DE-circRNAs (16 downregulated)

between the CRSwNP and control groups were obtained (Figure 2A–D, Supplementary Tables 1–4). As presented in the heatmap, the CRSwNP group exhibited decreased expression levels of LTF, BPIFB2, ZG16B, AZGP1, DMBT1, STATH, MUC5B, PPP1R1B, LPO, and LYZ, but elevated expression levels of CTAG2, CST1, CCL18, IGFBP3, HCRTR2, GOLGA6L1, UNC93A, SLITRK3, FAM71B, and SHH compared to the control group (Figure 2E–G).

Through prediction, we identified 5525 pairs of DE-miRNA-DE-lncRNA regulatory relationships. The lncRNA-miRNA-mRNA network contained 579 DEGs (including CSNK1A1L, CYP2U1, ATP13A1, ATP13A1, and ASPM), 57 miRNAs (including hsa-mir-519a-3p, hsa-mir-106b-5p, hsa-mir-20b-5p, and hsa-mir-92b-3p), and 29 lncRNAs (including SYNJ2-IT1, CBR3-AS1, INTS6-AS1, and FER1L6-AS2) (Supplementary Figure 1A). The hsa-let-7a-5p-AGO4 and other similar pairs were specific miRNA-mRNA pairs, while the hsa-let-7c-5p-CDKN2B-AS1 and others were miRNA-lncRNA pairs (Supplementary Table 5). Similarly, the circRNA-miRNA-mRNA network contained 16 DEGs (LRIG3 SFSWAP, STX3, ONECUT2, DNAJC6, ATP6V1B2, AGO4, CFL2, CRY2, LTA4H, BEND4, XBP1 SRCAP, ID1, PDGFB, and MTUS1), 3 miRNAs (hsa-let-7a-5p, hsa-let-7c-5p, and hsa-let-7g-5p), and 7 circRNAs (hsa_circ_0001009, hsa_circ_0000489, hsa_circ_0000799, hsa_circ_0000095, hsa_circ_0001725, hsa_circ_0000160, and hsa_circ_0000384) (Supplementary Figure 1B, Supplementary Table 6). After integrating the lncRNA-miRNA-mRNA and circRNA-miRNA-mRNA networks, we obtained the ceRNA network. This network comprised 46 DEGs (including AGO4, USP14, DNA2, PDGFB, and GP5), 3 miRNAs, 2 lncRNAs (LINC00885 and CDKN2B-AS1), and 7 circRNAs (hsa_circ_0001009, hsa_circ_0000489, hsa_circ_0000799, hsa_circ_0000095, hsa_circ_0001725, hsa_circ_0000160, and hsa_circ_0000384) (Figure 2H, Supplementary Table 7).

Enrichment Analysis of DEGs, DE-miRNAs, and DE-lncRNAs

Enrichment analysis indicated that the DEGs were associated with 613 GO terms and 42 KEGG pathways. The target genes of DE-miRNAs were associated with 566 GO terms and 53 KEGG pathways, while those of DE-lncRNAs target were associated with 601 GO terms and 42 KEGG pathways. The DEGs were mainly enriched in GO terms such as metal ion transmembrane transporter activity and actin-based cell projection (Figure 3A, Supplementary Table 8), and KEGG pathways such as protein digestion and absorption and synaptic vesicle cycle (Figure 3B, Supplementary Table 9). The target genes for DE-miRNAs were mainly enriched in GO terms such as mitotic cell cycle phase transition and nuclear division (Figure 3C, Supplementary Table 10), and in KEGG pathways such as the MAPK signaling pathway and cell cycle (Figure 3D, Supplementary Table 11). The target genes for DE-lncRNAs target genes were mainly enriched in GO terms such as metal ion transmembrane transporter activity and synaptic membrane (Figure 3E, Supplementary Table 12), and KEGG pathways such as glutamatergic synapse and protein digestion and absorption (Figure 3F, Supplementary Table 13).

Functional Enrichment Analysis of Candidate Genes

We used the 46 mRNAs in the ceRNA network as candidate genes for subsequent analyses. To further investigate the functions performed by these candidate genes, we performed functional enrichment analyses. The results indicated that the candidate genes were enriched in 419 GO terms and 5 KEGG pathways. The enriched GO terms included CRD-mediated mRNA stabilization, regulation of muscle cell differentiation, and meiotic spindle organization (Supplementary Figure 2, Supplementary Table 14). The GO biological process (BP) enrichment analysis identified several functional categories, primarily including the regulation of the miRNA metabolic process, RNA catabolic process, meiotic cell cycle, and myoblast differentiation, among others (Supplementary Figure 3A). KEGG enrichment highlighted key pathways, such as collecting duct acid secretion, microRNAs in cancer, and the p53 signaling pathway (Supplementary Figure 3B, Supplementary Table 15). The KEGG pathways were predominantly distributed across five major categories: human diseases, organismal systems, cellular processes, environmental information processing, and metabolism (Supplementary Figure 3C).

Screening and Performance Evaluation of Biomarkers

We constructed a PPI network based on 46 candidate genes, resulting in a network with 17 nodes and 16 edges, after excluding isolated proteins (Figure 4A). Subsequently, we identified five hub genes (EZH2, ASPM, IGF2BP3, HMGA2,

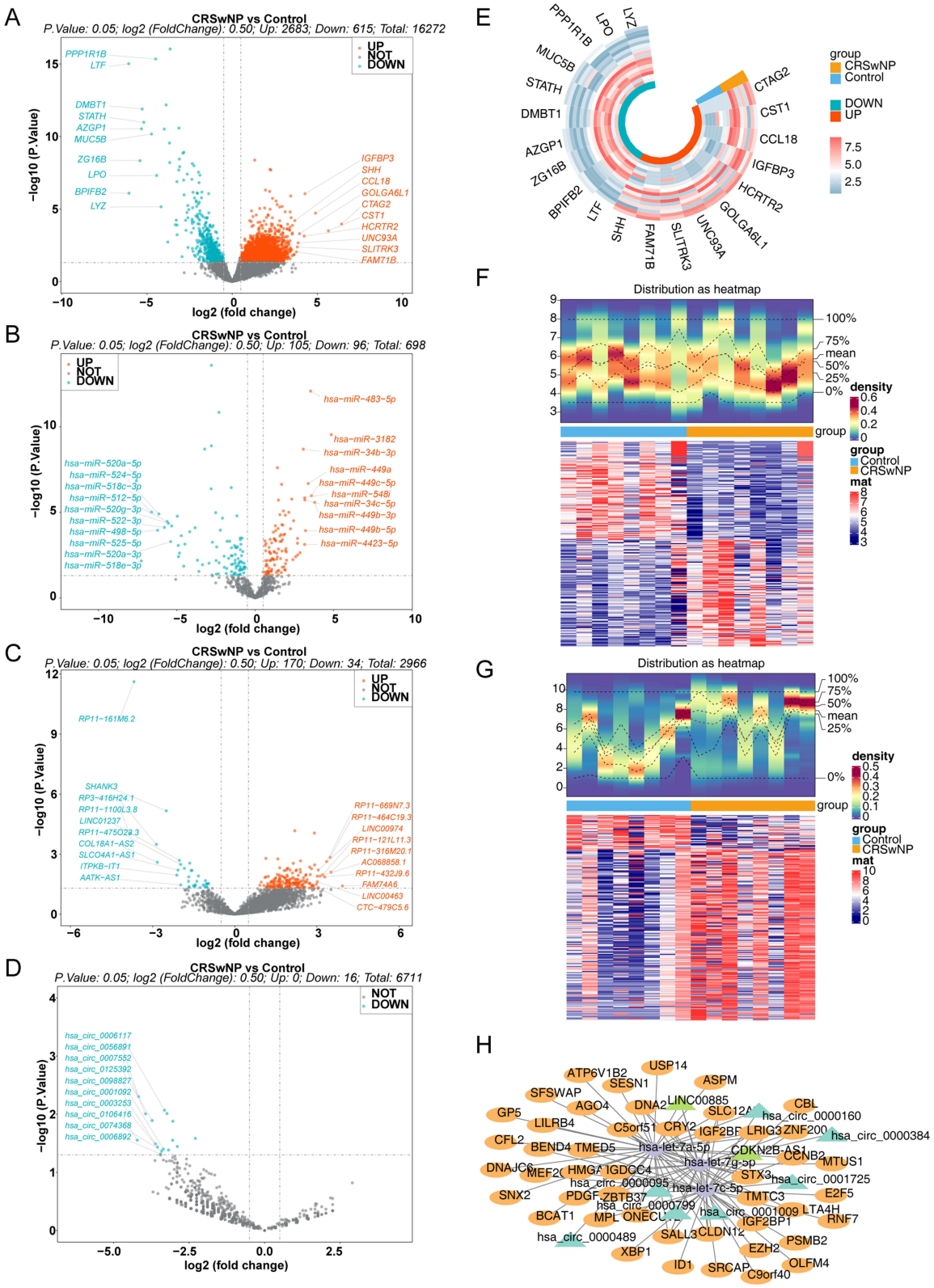

Figure 2 Identification of differentially expressed genes (DEGs), differentially expressed microRNAs (DE-miRNAs), differentially expressed-long non-coding RNAs (DE-lncRNAs), and differentially expressed-circular RNAs (DE-circRNAs). (**A**–**D**) Volcano plots of DEGs (**A**), DE-miRNAs (**B**), DE-lncRNAs (**C**), and DE-circRNAs (**D**). (**E**–**G**) Heatmaps of the DEGs (**E**), DE-miRNAs (**F**), and DE-lncRNAs (**G**). (**H**) Construction of competing endogenous RNAs (ceRNA) networks. Orange ovals, purple diamonds, dark green triangles, and light green triangles indicate mRNAs, miRNAs, circRNAs, and lncRNAs, respectively.

https://doi.org/10.2147/JIR.S525688

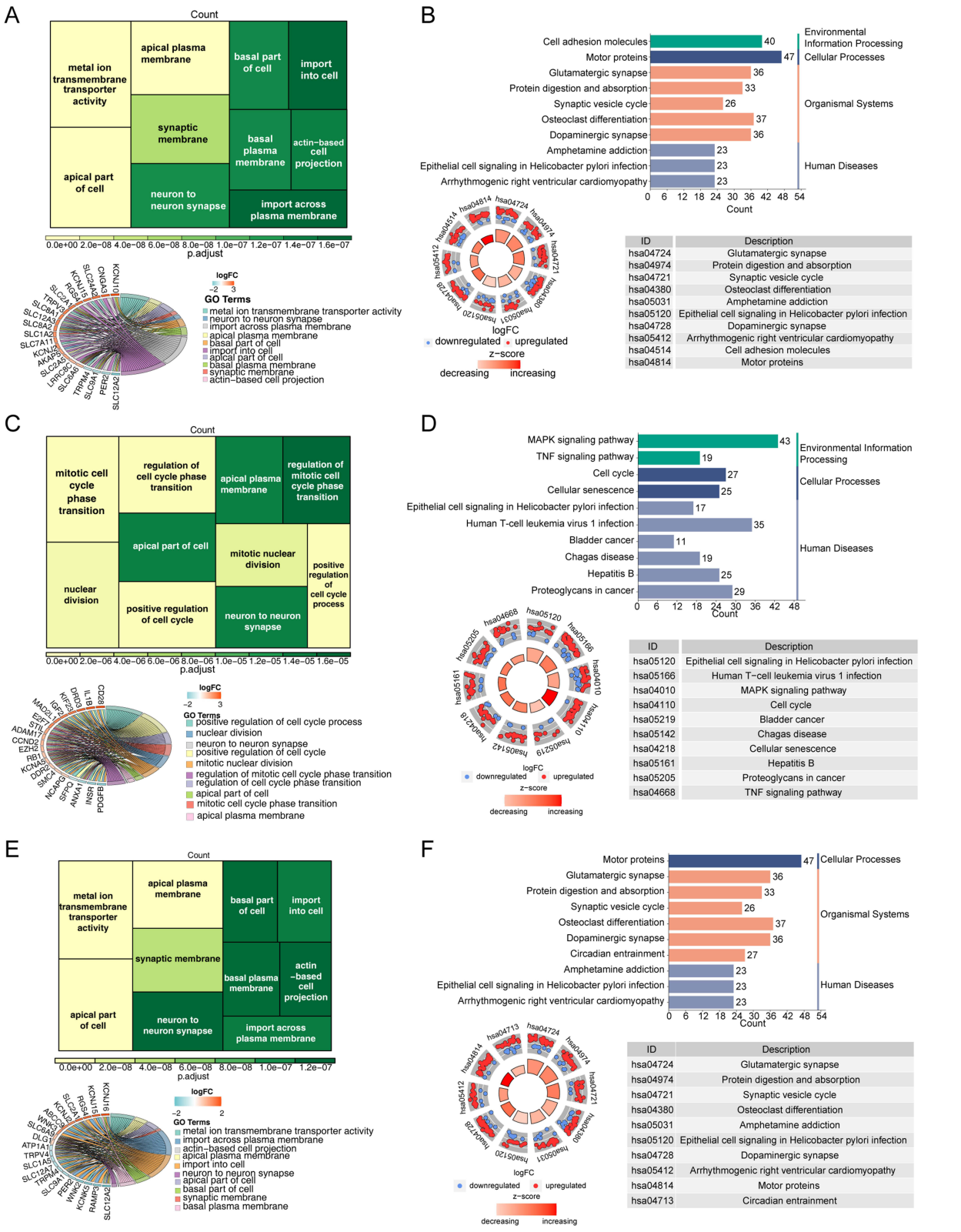

Figure 3 Results of the enrichment analysis of the differentially expressed genes (DEGs), differentially expressed microRNAs (DE-miRNAs), and differentially expressed-long non-coding RNAs (DE-lncRNAs). The relationship between DEGs (**A**), DE-miRNAs (**C**), DE-lncRNAs (**E**), and major terms annotated by Gene Ontology (GO) is indicated by the tree diagram and circos graph. The column plot and circle diagram of the top 10 Kyoto Encyclopedia of Genes and Genomes (KEGG) enrichment results for the DEGs (**B**), DE-miRNAs (**D**), and DE-lncRNAs (**F**).

and IGF2BP11) through further analysis using the plugin CytoHubba (Figure 4B). Moreover, using machine learning screening, we selected four SVM-RFE-feature genes (EZH2, IGF2BP3, HMGA2, and IGF2BP11) and four XGBoost-feature genes (IGF2BP1, EZH2, HMGA2, and ASPM) (Figure 4C and D). Subsequently, we overlapped these eight feature genes and identified three biomarkers (IGF2BP1, EZH2, and HMGA2) (Figure 4E).

The results of the ROC curves revealed that the area under the curve (AUC) values of the three biomarkers all exceeded 0.7, indicating that these genes had good diagnostic values (Figure 5A–C). Correlation analysis revealed a significantly positive correlation between *EZH2* and *HMGA2* (Figure 5D). Moreover, the ANN analysis revealed that the optimal number of hidden neuron layers was three (Figure 5E). Notably, *HMGA2* was the most influential variable affecting the predictive outcomes of the model (Figure 5F). The confusion matrix indicated that the model achieved 100% accuracy, while the ROC curve further indicated good stability (AUC = 0.719) (Figure 5G–H).

Single-Gene GSEA and Immune-Related Analyses of Biomarkers

After constructing the ANN network, we analyzed the function of the biomarkers. The enrichment results indicated that the biomarkers were mainly enriched in KEGG terms such as neuroactive ligand-receptor interaction and olfactory transduction (Figure 6A–C, Supplementary Table 16–18). We further analyzed the differences in the proportions of immune factors between the CRSwNP and control groups. In total, one immune cell type (monocytes), three chemokines (CCL18, CCL28, and CXCL17), and one MHC (HLA-DOA) were significantly different between the CRSwNP and control groups (Figure 6D–F). Moreover, correlation analysis of biomarkers with differential immune factors revealed that HMGA2 had the strongest negative association with CXCL17, whereas IGF2BP1 exhibited the strongest positive relationship with HLA-DOA (Figure 6G).

Establishment of TF-mRNA Regulatory Networks, Regulatory Axes, and Diseases Associated with Biomarkers

To identify mRNA-TF networks of biomarkers in CRSwNP, we used the online databases ChEA3 and NetworkAnalyst, identifying a total of 106 TFs associated with the biomarkers. Subsequently, we established an mRNA-TF regulatory network containing 109 nodes (3 biomarkers) and 106 TFs (including CCND1, E2F6, OLIG2, and TEAD4) (Supplementary Figure 4A). In the DGIDB database, we identified one biomarker (EZH2) targeted by seven therapeutic drugs (doxorubicin, vorinostat, selumetinib, MK-2206, CPI-1205, tazemetostat, and dabrafenib) (Supplementary Figure 4B).

The ceRNA sub-network of biomarkers contained 3 mRNAs (EZH, HMGA2, and IGF2BP1), 12 miRNAs (including hsa-mir-485-5p, hsa-mir-98-5p, and hsa-let-7c-5p) and 9 lncRNAs (including CASC2, CDKN2B-AS1, and DUXAP8) (Supplementary Figure 4C). Correlation analysis of biomarkers with ENT diseases revealed that both IGF2BP1 and EZH2 were highly correlated with allergic rhinitis, while HMGA2 was highly associated with nose neoplasms (Supplementary Figure 4D).

Validation of the Expression of the Biomarkers

Expression validation results from the TS-CRSwNP dataset indicated that the three biomarkers significantly differed between control and CRSwNP tissues, with high expression levels in the CRSwNP group (Figure 6H). The results obtained using the validation cohort were consistent with those observed in the TS-CRSwNP dataset, except for IGF2BP1 (Figure 6I).

Experimental Verification

We further assessed the protein expression levels of the three biomarkers (IGF2BP1, EZH2, and HMGA2) in samples obtained from 20 patients with CRSwNP and 20 control participants using IHC analysis. The results indicated that IGF2BP1 expression was predominantly located in the cytoplasm, EZH2 was mostly expressed in the cytoplasm, while HMGA2 was expressed both in the cytoplasm and the nucleus. A subsequent quantitative analysis revealed that the

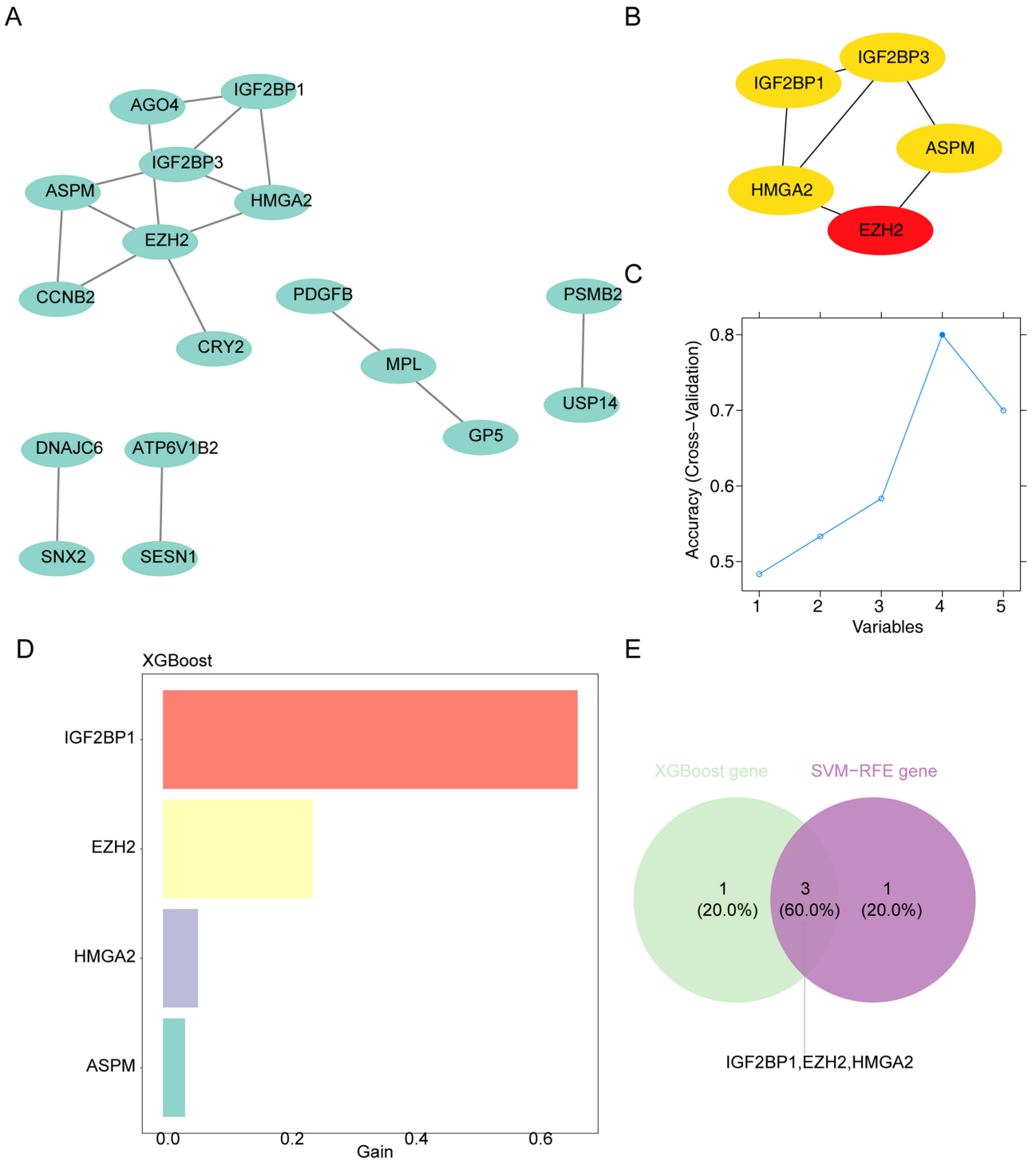

Figure 4 Screening of the three biomarkers. (**A**) Construction of the protein–protein interaction (PPI) network of 17 proteins. Each green circle represents a protein, while the gray lines represent the interaction relationships between proteins. (**B**) Construction of the core network with genes of TOP 5 degree value. The intensity of the red color indicates a higher degree value of the protein node. (**C**) Construction of Support vector machines-recursive feature elimination (SVM-RFE) models for the five candidate genes. (**D**) Column plot of genetic coefficient for the 4 XGBoost-feature genes. (**E**) Venn diagram of the four SVM-RFE-feature genes and four XGBoost-feature genes.

number of cells positive for EZH2 ($p < 0.01$; Figure 7A), HMGA2 ($p < 0.0001$; Figure 7B), and IGF2BP1 ($p < 0.001$; Figure 7C) expression was significantly higher in the CRSwNP group than in the control group.

We then performed qRT-PCR to validate our findings by assessing the mRNA expression levels of IGF2BP1, EZH2, and HMGA2 in 15 CRSwNP samples and 15 control samples. The results revealed that the mRNA expression levels of

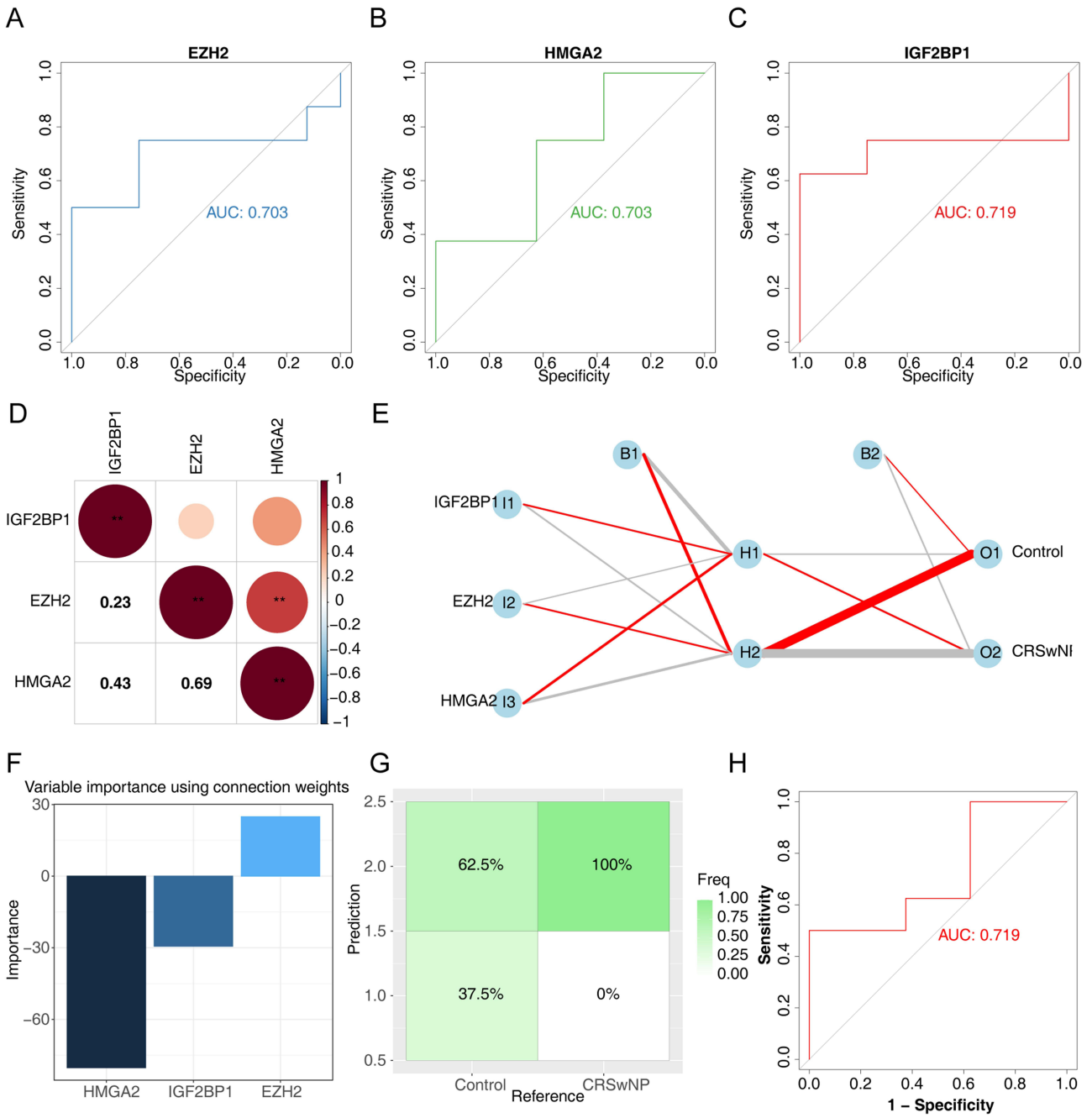

Figure 5 Performance evaluation of the three biomarkers. (**A**–**C**) Receiver operating characteristic (ROC) curves of the enhancer of zeste homolog 2 (EZH2) (**A**), the high-mobility gene group A2 (HMGA2) (**B**), and Insulin-like growth factor 2 mRNA-binding protein 1 (IGF2BP1) (**C**). The horizontal axis represents specificity, and the vertical axis represents sensitivity. The area under the curve (AUC) represents the accuracy (prediction performance). (**D**) Correlation analysis of the three biomarkers. (**E**) Construction of the artificial neural network (ANN) for 3 biomarkers. The colors of the lines represent positive and negative contributions, with red representing a positive contribution and gray a negative contribution. (**F**) Importance of the independent variables on the predicted results of the model. The horizontal coordinate is the hub gene, and the vertical coordinate represents the importance of the gene to the model outcome. (**G** and **H**) Confusion matrix (**G**) and ROC curve (**H**) for the three biomarkers.

EZH2 ($p < 0.05$; Figure 7D), HMGA2 ($p < 0.01$; Figure 7E), and IGF2BP1 ($p < 0.01$; Figure 7F) were significantly higher in the CRSwNP group than in the control group.

To further elucidate the molecular mechanism by which EZH2 regulates HMGA2 expression, we downregulated EZH2 expression. Specifically, we synthesized three siRNAs targeting EZH2 mRNA sequences and transfected them into HNEpCs. As presented in Figure 8A, siEZH2-1 exhibited more potent inhibition, resulting in a more pronounced downregulation of EZH2 expression. We measured the mRNA levels of H3k27me3 and HMGA2 using qRT-PCR.

https://doi.org/10.2147/JIR.S525688

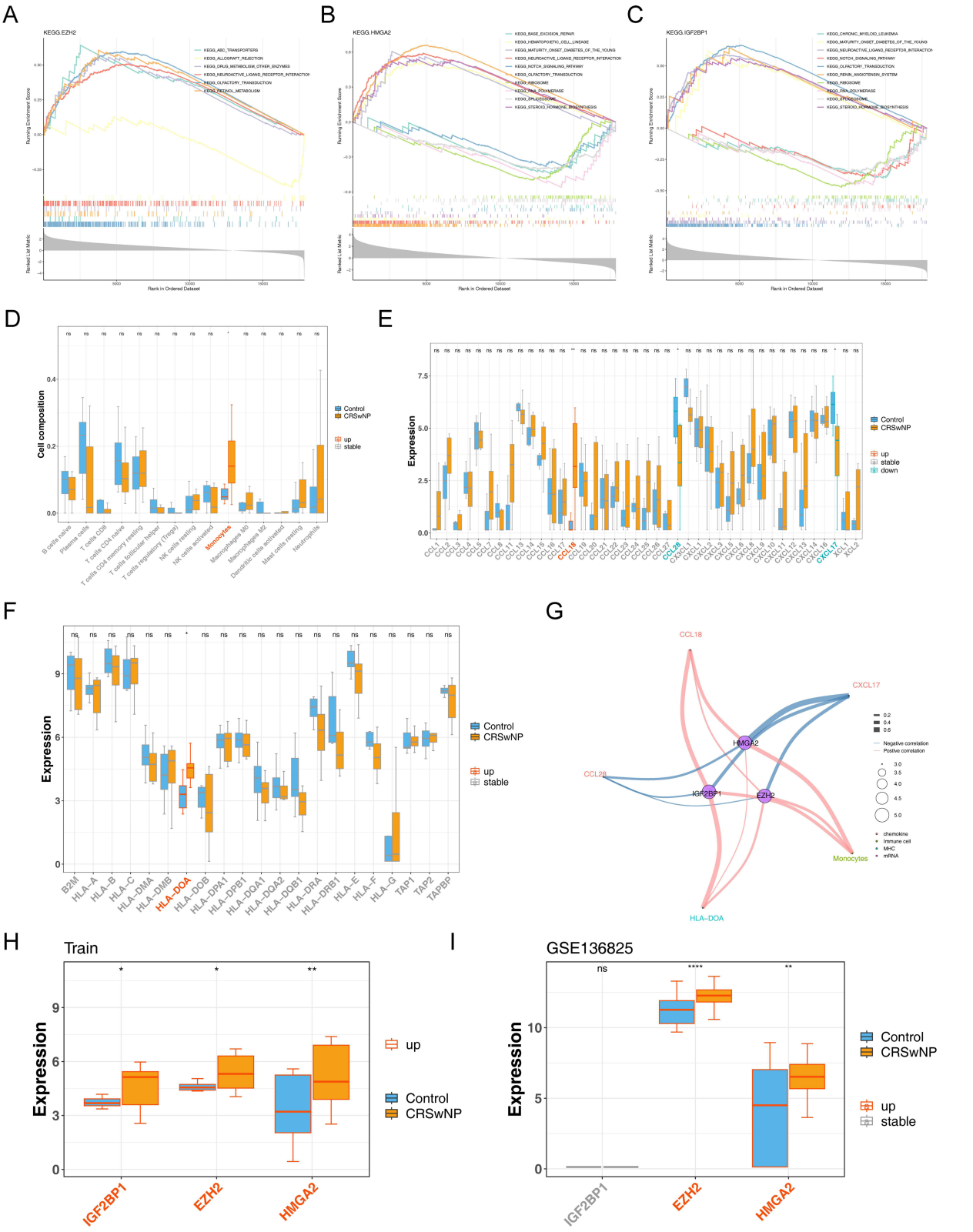

Figure 6 Single-gene Gene Set Enrichment Analysis (GSEA) and immune-related analyses of the three biomarkers. (**A**–**C**) Single-gene GSEA of EZH2 (**A**) HMGA2 (**B**), and IGF2BP1 (**C**). (**D**) Differences in the abundance of immune cells between the CRSwNP and control groups. *p < 0.05. (**E**) Differences in chemokine expression between the CRSwNP and control groups. *p < 0.05, **p < 0.01. (**F**) Differences in MHC expression between the CRSwNP and control groups. *p < 0.05. (**G**) Correlation analysis of biomarkers with differential immune factors. (**H**) Expression of the three biomarkers in the training dataset. *p < 0.05, **p < 0.01. (**I**) Expression of three biomarkers in the GSE136825 dataset. **p < 0.01, ****p < 0.0001.

Abbreviation: ns, not significant.

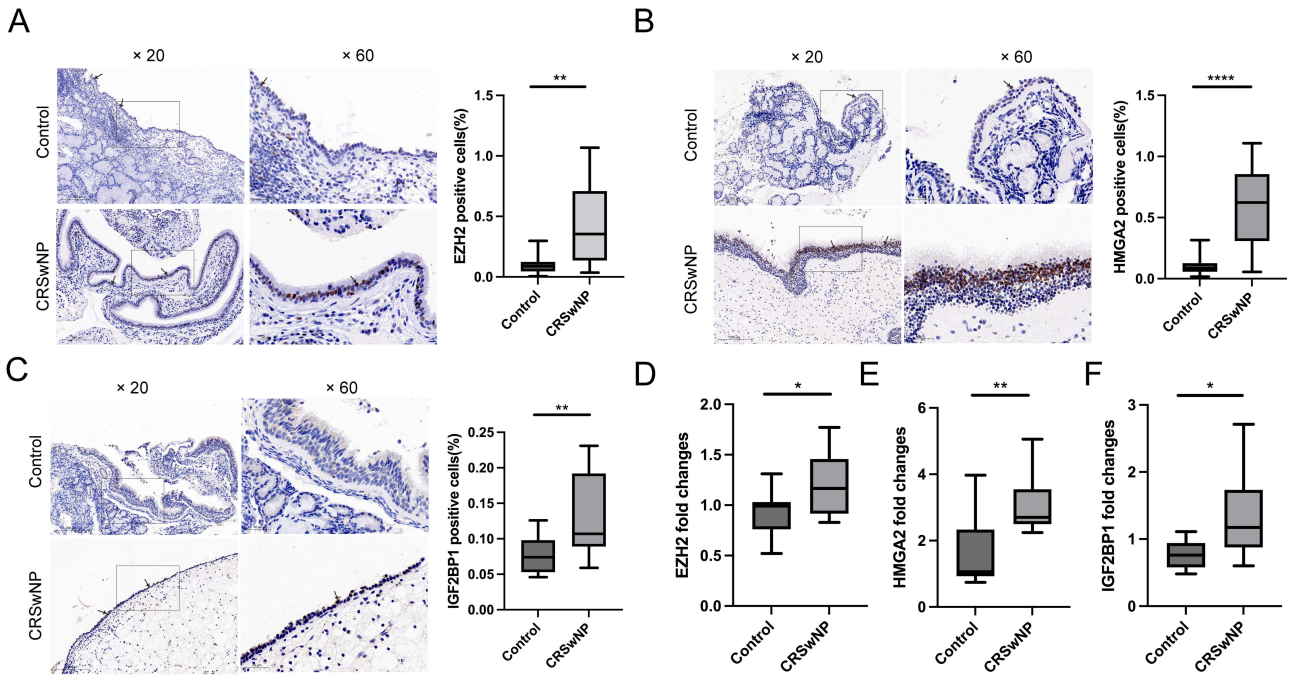

Figure 7 Quantification of EZH2, HMGA2, and IGF2BP1 expression. (**A**) Representative immunohistochemical (IHC) staining images and quantification of EZH2 levels in the control and CRSwNP group (Student's *t*-test, n =20 per group). The boxes show high-power images (×60) obtained from low-power images (×20). The black arrows indicate EZH2. The scale bar on the left image is 200 μm, and the scale bar on the right image is 50 μm. **p < 0.01. (**B**) Representative IHC staining images and quantification of HMGA2 levels in the control and CRSwNP group (Student's *t*-test, n =20 per group). The boxes show high-power images (×60) obtained from low-power images (×20). The black arrows indicate HMGA2. The scale bar on the left image is 200 μm, and the scale bar on the right image is 50 μm. ****p < 0.0001. (**C**) Representative IHC staining images and quantification of IGF2BP1 levels in the control and CRSwNP groups (Student's *t*-test, n =20 per group). The boxes show high-power images (×60) obtained from low-power images (×20). The black arrows indicate EZH2. The scale bar on the left image is 200 μm, and the scale bar on the right image is 50 μm. **p < 0.01. (**D**) Expression of EZH2 in the control and CRSwNP groups (Student's *t*-test, n =15 per group). *p < 0.05. (**E**) Expression of HMGA2 in the control and CRSwNP groups (Student's *t*-test, n =15 per group). **p < 0.01. (**F**) Expression of IGF2BP1 in the control and CRSwNP groups (Student's *t*-test, n =15 per group). *p < 0.05.

Following the downregulation of EZH2 expression, the expression level of H3k27me3 increased, whereas that of HMGA2 decreased in HNEpCs (Figure 8B and C). We further used IF to detect changes in the protein expression profile of H3k27me3 and HMGA2 after the downregulation of EZH2. We semi-quantitatively scored the immunofluorescence results to assess the correlation between reduced EZH2 expression levels and the expression of H3k27me3 and HMGA2. The figure presents representative images of H3k27me3 and HMGA2 expression after the downregulation of EZH2 expression in HNEpCs, revealing that this downregulation resulted in increased H3k27me3 expression levels (Figure 8D) and decreased HMGA2 expression levels (Figure 8E).

To assess the effects of the upregulation of EZH2 expression, we synthesized three plasmids overexpressing EZH2 and transfected them into HNEpCs. Figure 9A demonstrates that the OE-EZH2 plasmid exhibited a stronger effect, resulting in more significant EZH2 overexpression than that induced by the two other plasmids. We used qRT-PCR to detect the mRNA levels of H3k27me3 and HMGA2 in response to EZH2 upregulation. Following the upregulation of EZH2 expression, the expression level of H3k27me3 was significantly decreased, whereas that of HMGA2 was increased (Figure 9B and C). We used IF to identify changes in the protein expression patterns of H3k27me3 and HMGA2 following the upregulation of EZH2. In HNEpCs with upregulated EZH2 expression, H3k27me3 expression levels were decreased (Figure 9D) whereas those of HMGA2 were increased (Figure 9E). These results confirm that EZH2 promotes HMGA2 expression by downregulating H3k27me3 expression and inhibits HMGA2 expression by upregulating H3k27me3 expression in HNEpCs.

Discussion

In the present study, we performed RNA-seq using CRSwNP and control tissues, enabling the identification of candidate genes and pathways associated with the disease. Pathway analysis revealed key signaling pathways involved in the

https://doi.org/10.2147/JIR.S525688

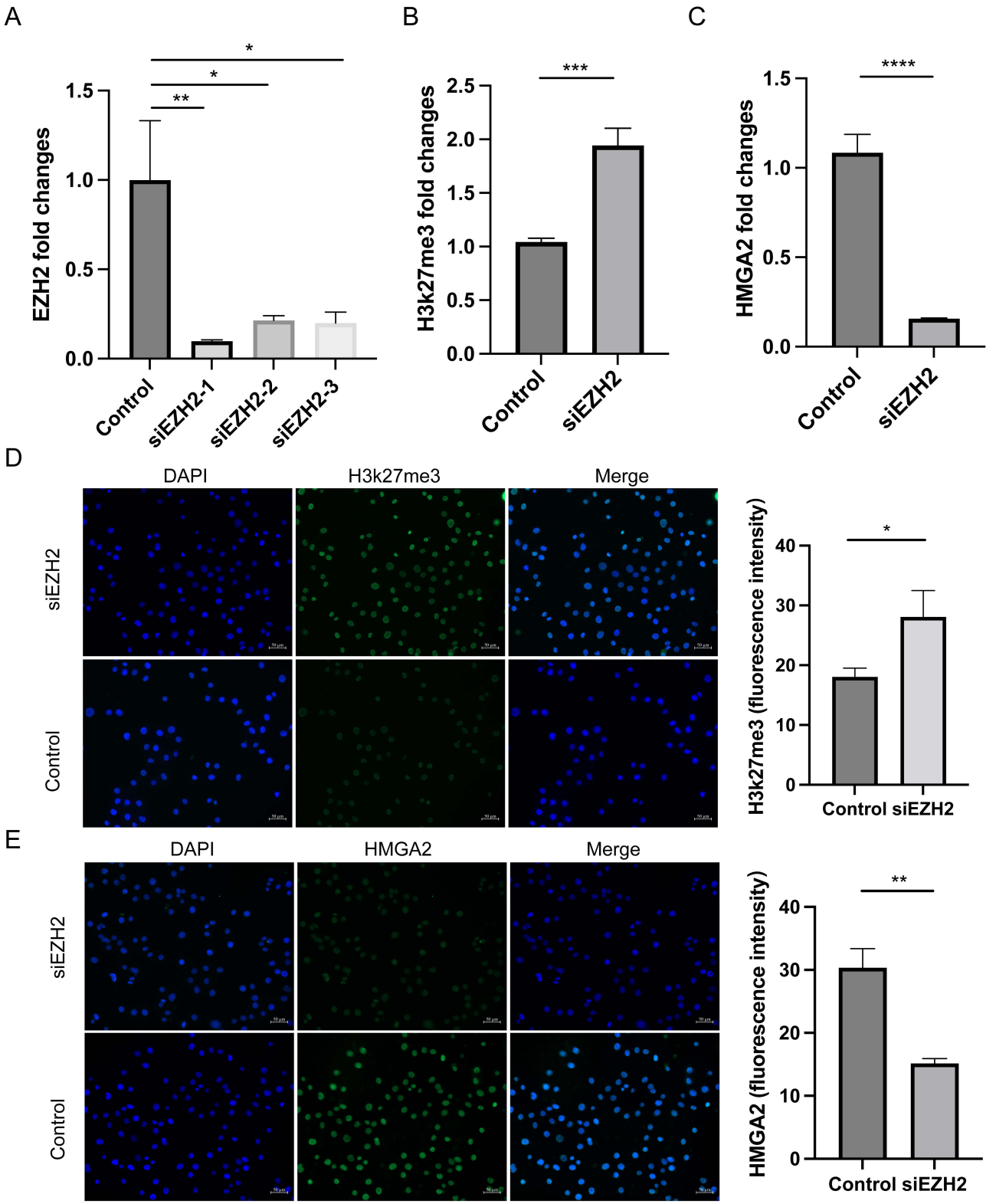

Figure 8 Immunofluorescence analysis of EZH2, HMGA2, and IGF2BP1 expression based on three different siRNAs targeting EZH2 mRNA sequence. (**A**) Expression of EZH2 in the control group and HNEpCs transfected with three different siRNAs targeting EZH2 mRNA sequences. *p < 0.05, **p < 0.01. (**B**) Expression of H3k27me3 in the control group and HNEpCs transfected with siEZH2. ***p < 0.001. (**C**) Expression of HMGA2 in the control group and HNEpCs transfected with siEZH2. ****p < 0.0001. (**D**) Representative immunofluorescence images and quantified data showing the expression of H3k27me3 in the control group and HNEpCs transfected with siEZH2. Nuclei were stained with DAPI. Scale bar = 50 μm. *p < 0.05. (**E**) Representative immunofluorescence images and quantified data showing the expression of H3k27me3 in the control cell and HNEpCs transfected with siEZH2. Nuclei were stained with DAPI. Scale bar = 50 μm. **p < 0.01.

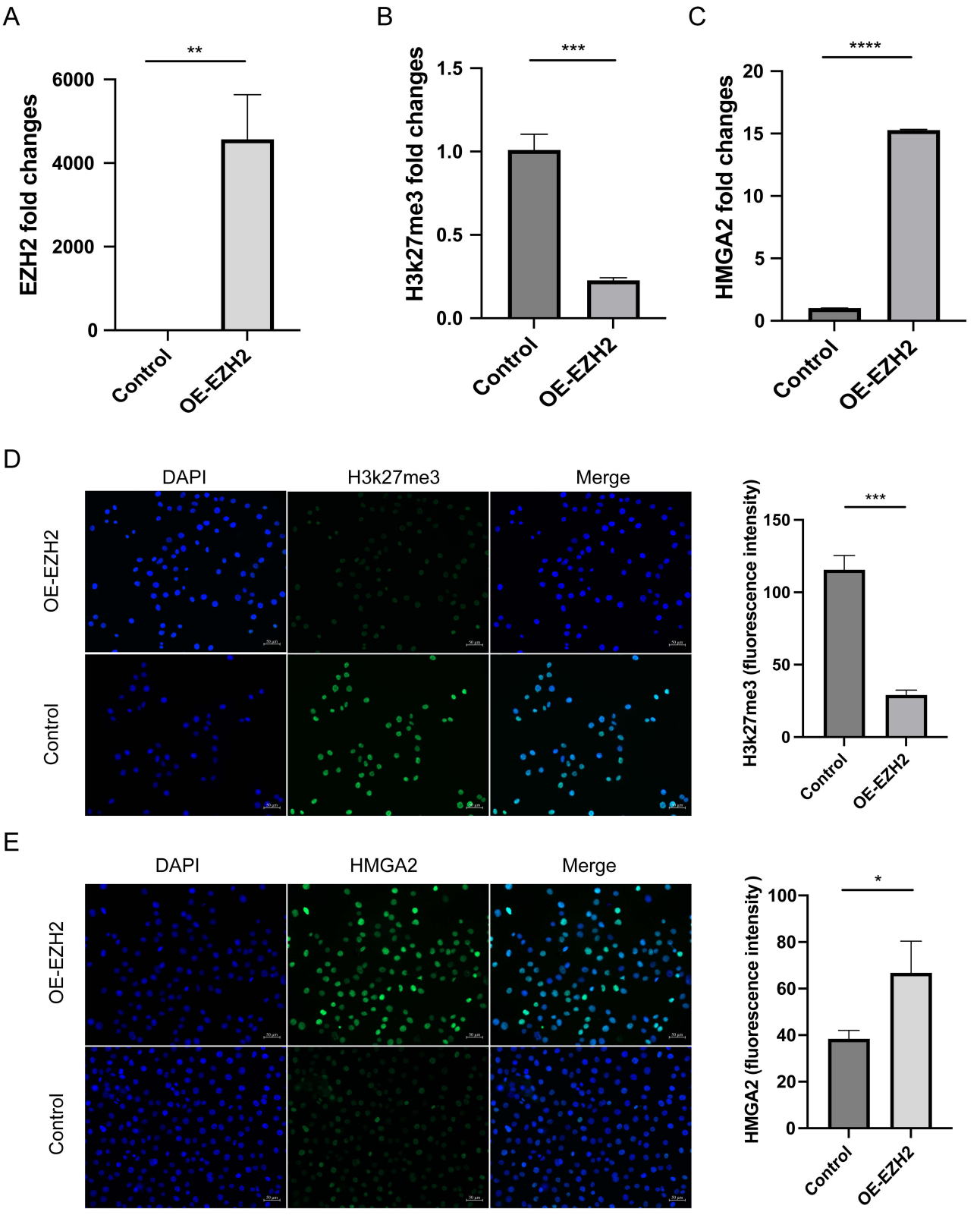

Figure 9 Immunofluorescence analysis of EZH2, HMGA2, and IGF2BP1 expression based on three different plasmids overexpressing (OE) EZH2. (**A**) Expression of EZH2 in the control group and HNEpCs transfected with three different plasmids overexpressing (OE) EZH2. **p < 0.01. (**B**) Expression of H3k27me3 in the control group and HNEpCs transfected with OE-EZH2. ***p < 0.001. (**C**) Expression of HMGA2 in the control group and HNEpCs transfected with OE-EZH2. ****p < 0.0001. (**D**) Representative immunofluorescence images and quantified data showing the expression of H3k27me3 in the control group and HNEpCs transfected with OE-EZH2. Nuclei were stained with DAPI. Scale bar = 50 μm. ***p < 0.001. (**E**) Representative immunofluorescence images and quantified data showing the expression of H3k27me3 in the control group and HNEpCs transfected with OE-EZH2. Nuclei were stained with DAPI. Scale bar = 50 μm. *p < 0.05.

https://doi.org/10.2147/JIR.S525688

pathogenesis of CRSwNP. Comparison of CRSwNP tissues with control ones revealed alterations in key signaling pathways such as metal ion transmembrane transporter activity and MAPK signaling pathway, which are associated with chronic airway inflammation.[39,40] The identified DEGs, target genes of DE-miRNAs, and DE-target genes of lncRNAs were also enriched in pathways related to metal ion transmembrane transporter activity and MAPK signaling. Notably, we identified three biomarkers (IGF2BP1, EZH2, and HMGA2) that are closely associated with CRSwNP.

IGF2BP1 is a key regulator of mRNA metabolism and transport during organismal development. It is primarily expressed in embryos, with relatively low expression in adults and healthy tissues.[41] Mechanistically, IGF2BP1 binds to the methyl group of RNA to stabilize it and prevent its degradation, thereby promoting protein translation. Functionally, IGF2BP1 plays an important role in regulating development and cell proliferation.[42] Consistent with previous studies, we observed that *IGFBP1* was highly expressed in the CRSwNP group compared to the control group. The observed differences in IGF2BP1 expression between the training and validation sets in this study may stem from multiple factors. Variations in sample collection, processing, and storage protocols, as well as differences in experimental equipment, could all contribute to expression level discrepancies. Additionally, individual variations such as age, sex, disease status, and lifestyle factors may influence IGF2BP1 expression, and the demographic differences between subjects in the training and validation sets might have amplified this effect.

The EZH2 gene is the human homolog of the Drosophila zeste gene enhancer and belongs to the family of epigenetic regulators.[43] EZH2 performs two main biological functions, depending on polycomb group genes (PcGs). Specifically, it plays a role in various biological processes, and its expression is associated with cancer onset, progression, metastasis, metabolism, drug resistance, and immune modulation. Therefore, EZH2 has become a potential target for immunotherapy.[44] In allergic rhinitis, EZH2 can promote Th1 cell differentiation or inhibit Th2 cell differentiation, thereby exacerbating the pathological process of the disease.[27] Furthermore, EZH2 may play a pro-inflammatory role in allergic airway inflammation, as inhibiting its expression can alleviate allergic airway inflammation.[26] Consistent with findings in other immune-related diseases, in our study, EZH2 was highly expressed in nasal polyp tissues, suggesting that EZH2 plays an important role in the pathogenesis of CRSwNP. In general, EZH2 expression is suppressed through epigenetic modifications, leading to the inhibition of the transcription of target genes, a mechanism that has received considerable attention in tumor research.[45] In this study, we focused on the role of EZH2 in NPs. EZH2 is involved in the regulation of inflammation,[46] potentially playing a role in the pathophysiology of chronic sinusitis with NPs. Notably, inhibiting EZH2 significantly reduces inflammation and lung injury in acute lung injury (AKI) induced by sepsis.[47] EZH2 inhibition can alleviate AKI induced by ischemia-reperfusion and reduce the associated inflammatory responses.[48]

HMGA2 is a transcriptional regulator essential for embryonic development, with its expression decreasing during postembryonic stages.[49] However, it is often re-expressed during tumorigenesis.[50] RNA-sequencing analyses of clinical and normal samples indicate that HMGA2 expression is upregulated in many cancers.[51] HMGA2 induces cancer cell proliferation by promoting the transition into the S phase of the cell cycle, inhibiting apoptosis, and inducing DNA repair. In addition, HMGA2 regulates miRNA expression by activating multiple signaling pathways, including the MAPK/ERK, TGFβ/Smad, PI3K/AKT/mTOR/NFKB, and RKIP pathways.[49] In our study, EZH2 and HMGA2 were highly expressed and synergistic, suggesting that these two key genes may collaboratively play an important role in the pathogenesis of CRSwNP.

Epigenetic abnormalities are important factors contributing to the development of various diseases.[52] Histone modifications in chromosomes, which serve as key markers of epigenetic inheritance, are critical in regulating the transcription of disease-associated genes by controlling their expression.[24] EZH2, a prominent epigenetic target, is a histone methyltransferase that can affect cellular functions by catalyzing the trimethylation of histone H3 lysine 27 (H3K27). Its expression has been detected in HNEpCs.[53] In our study, we found that, similar to findings in tumor tissues, EZH2 overexpression in HNEpCs decreased the methylation level of H3K27, whereas EZH2 downregulation increased the methylation level of H3K27. Recent advances in immunotherapy have highlighted the importance of the immune system in disease control, but only a minority of patients currently benefit. Studies have shown that targeting epigenetic factors that inhibit immune cell function, such as EZH2 inhibition, can improve the efficacy of immunotherapy by reshaping the disease microenvironment and enhancing the coordination of the immune system.[54,55] In addition, lncRNA PiHL inhibits its localization in HMGA2 promoter region by binding to EZH2, thereby reducing H3K27me3 methylation

level and promoting HMGA2 expression.[56] In our study, we found that HMGA2 exhibited a strong synergistic effect with EZH2. Specifically, when EZH2 was overexpressed, H3K27me3 expression was downregulated whereas HMGA2 expression was upregulated. In contrast, downregulated EZH2 expression resulted in increased H3K27me3 levels and decreased HMGA2 expression. These results suggest that targeting EZH2 may pave the way for enhancing immune surveillance in CRSwNP. We also found that EZH2 and HMGA2 were co-regulated by hsa-let-7c-5p. We speculated that hsa-let-7c-5p may promote the high expression of EZH2 through histone modification, and then activate the expression of HMGA2 in CRSwNP through a more complex regulatory mechanism, revealing the potential interaction between EZH2 and HMGA2. It is now increasingly understood that CRS phenotypes do not necessarily match these classic endotypic presumptions, and the underlying pathogenetic processes in CRS may encompass type 1, type 2, or type 3 inflammation, or a mix. However, from the perspective of epigenetics, genetic predisposition is stronger in patients with CRS with nasal polyps compared with those without nasal polyps (CRSsNP).[57] Among the many epigenetic regulatory modalities, methylation modification of histone H3 at its K27 position mediates the silencing of gene expression, and EZH2 is a key enzyme molecule that induces methylation modification of H3K27.[58] Furthermore, the three biomarkers (IGF2BP1, EZH2, and HMGA2) demonstrate significant correlations with the differential chemokine CCL18. Studies have revealed that CCL18 is highly expressed in M2 macrophages and aligns with the immune characteristics of type 2 inflammatory endotypes, suggesting its potential critical role in type 2 inflammation.[59] Dysregulation of EZH2 is closely associated with CRSwNP. HMGA2 could synergize with EZH2 to induce epithelial cell destruction; therefore, the study of the immunomodulatory role of EZH2 and the related epigenetic regulatory mechanism is of great significance for the prevention and diagnosis of related immune disease. We further hypothesize that IGF2BP1, EZH2, and HMGA2 may play pivotal roles in type 2 inflammatory endotypes of CRSwNP through epigenetic regulatory mechanisms. These genes likely interact and modulate chemokine expression (eg, CCL18) via their coordinated actions in specific immune cells, thereby promoting the initiation and perpetuation of type 2 inflammatory responses.

The EZH2 signaling pathway, known as a driver of cancer progression, can potentially interfere with anti-tumor immune responses, making it an important therapeutic target for cancer therapy.[60] In this study, seven small molecule drugs were selected based on the prediction of EZH2. VORINOSTAT, as a histone deacetylase inhibitor, affects gene expression by regulating chromatin accessibility and has been widely used in the treatment of hematological malignancies.[61] TAZEMETOSTAT is a potent targeted epigenetic regulator that specifically inhibits EZH2.[62] A previous study on the correlation between EZH2-driven tumor cells and immune response has indicated that inhibiting EZH2 exhibits a synergistic effect when combined with immunotherapy and chemotherapy drugs.[63] Moreover, EZH2 inhibitors have demonstrated potential in overcoming immunotherapy resistance, with preliminary exploration of combined EZH2 inhibition and immunotherapy showing efficacy in certain solid tumors and lymphomas.[64,65] However, it should be noted that EZH2 inhibition may influence the effects of existing immunotherapies by modulating the tumor microenvironment (TME), though the precise mechanisms remain incompletely understood and require further validation.[66] While EZH2 inhibitors may offer novel combination opportunities with immunotherapy, optimal integration strategies with current immunotherapeutic approaches demand thorough investigation. Clinically, common adverse effects of EZH2 inhibitors include fatigue, upper respiratory infections, musculoskeletal pain, nausea, and abdominal pain, with vigilance required for potential severe reactions.[67] These preliminary findings regarding both therapeutic efficacy and safety profiles necessitate additional clinical trials to confirm the safety and effectiveness of EZH2 inhibitors when combined with immunotherapeutic agents.

Limitations

Despite significant findings, this study has limitations. The RNA-seq analysis in this study was conducted with a relatively small sample size (n=8 per group). While we have partially mitigated this limitation through external validation and functional experiments, the modest sample size may constrain the statistical power of our findings. Increasing the sample size can enhance statistical reliability,[68] leading to improved estimation accuracy and significance, but practical constraints such as cost and time must be taken into account. To address these limitations and further validate our findings, future studies will aim to reduce selection bias by enlarging the sample size, combining sampling methods, and collecting auxiliary information.[69,70] Furthermore, since a single cell line may not adequately represent the

complexity of CRSwNP, future studies should incorporate more in vivo functional experiments and expand sample sizes to cover different inflammatory endotypes, thereby further exploring the epigenetic role of EZH2 in CRSwNP.

Conclusion

Our study has important clinical implications. Based on a comparison of tissues collected from patients with CRSwNP and controls, our RNA-seq analysis identified three biomarkers and their associated signaling pathways and gene sets. This approach minimizes false positive findings arising from interactions between environmental and genetic factors. In addition, the continuous accumulation of immune tolerance provides new targets for the treatment of CRSwNP, suggesting that immunomodulators may play a role in the treatment of the disease. Nonetheless, given the complexity of clinical application, our findings should be further validated and cautiously evaluated for their translational potential. Future research should focus on exploring how to integrate these molecular mechanisms into the diagnostic or therapeutic framework, such as developing EZH2-based biomarker detection methods and exploring the application potential of EZH2 inhibitors in the treatment of CRSwNP, so as to provide clearer and powerful guidance for clinical practice.

Abbreviations

ceRNAs, competing endogenous RNAs; CRSwNP, chronic rhinosinusitis with nasal polyps; EZH2, The Enhancer of zeste homolog 2; DEGs, differentially expressed genes; DE-miRNAs, differentially expressed microRNAs; DE-lncRNAs, differentially expressed-long non-coding RNAs; DE-circRNAs, differentially expressed-circular RNAs; TS-CRSwNP, transcriptomic sequencing CRSwNP; PPI, protein–protein interaction; ScRNA-seq, Single-cell RNA-sequencing; IHC, immunohistochemistry; qRT-PCR, quantitative real-time reverse transcription polymerase chain reaction; WB, Western blot; IF, immunofluorescence; CRS, Chronic rhinosinusitis; CRSsNP, CRS without nasal polyps; ILC, intrinsic lymphoid cell; RNA-seq, RNA-sequencing; NP, nasal polyps; GEO, Gene Expression Omnibus; GO, Gene Ontology; KEGG, Kyoto Encyclopedia of Genes and Genomes; ROC, receiver operating characteristic; ANN, Artificial Neural Network; GSEA, Gene set enrichment analysis; MHC, histocompatibility complex; TF, transcription factors; ENT, ear-nose-throat; CTD, Comparative Toxicogenomics; PCA, principal component analysis; HNEpCs, human nasal epithelial cells; BP, biological process; CC, cellular component; MF, molecular function; SVM-RFE, Support vector machines-recursive feature elimination; AUC, area under the curve; HMGA2, high-mobility gene group A2; IGF2BP1, Insulin-like growth factor 2 mRNA-binding protein 1.

Ethics Approval and Informed Consent

All procedures involving human participants were performed in accordance with the Declaration of Helsinki and approved by the Institutional Review Board (2022-department-564) of the Ethics Committee of Beijing Chaoyang Hospital. All the participants provided written informed consent before participating in the trial.

Funding

This research was funded by the Clinical Research Incubation Project, Beijing Chao-Yang Hospital, Capital Medical University (CYFH202211).

Disclosure

The authors report no conflicts of interest in this work.

References

1. Kato A, Peters AT, Stevens WW, Schleimer RP, Tan BK, Kern RC. Endotypes of chronic rhinosinusitis: relationships to disease phenotypes, pathogenesis, clinical findings, and treatment approaches. *Allergy*. 2022;77(3):812–826. doi:10.1111/all.15074
2. Kato A, Schleimer RP, Bleier BS. Mechanisms and pathogenesis of chronic rhinosinusitis. *J Allergy Clin Immunol*. 2022;149(5):1491–1503. doi:10.1016/j.jaci.2022.02.016
3. Akdis CA, Bachert C, Cingi C, et al. Endotypes and phenotypes of chronic rhinosinusitis: a PRACTALL document of the European Academy of Allergy and Clinical Immunology and the American Academy of Allergy, Asthma & Immunology. *J Allergy Clin Immunol*. 2013;131(6):1479–1490.

4. Marin C, Hummel T, Liu Z, Mullol J. Chronic rhinosinusitis and COVID-19. *J Allergy Clin Immunol Pract*. 2022;10(6):1423–1432.
5. Ahern S, Cervin A. Inflammation and endotyping in chronic rhinosinusitis-a paradigm shift. *Medicina*. 2019;55(4):95.
6. Bachert C, Maurer M, Palomares O, et al. What is the contribution of IgE to nasal polyposis? *J Allergy Clin Immunol*. 2021;147(6):1997–2008.
7. Senna G, Micheletto C, Piacentini G, et al. Multidisciplinary management of type 2 inflammatory diseases. *Multidiscip Respir Med*. 2022;17 (1):813.
8. De Corso E, Baroni S, Onori ME, et al. Calprotectin in nasal secretion: a new biomarker of non-type 2 inflammation in CRSwNP. *Acta Otorhinolaryngol Ital*. 2022;42(4):355–363.
9. Saeidian AH, Youssefian L, Vahidnezhad H, Uitto J. Research techniques made simple: whole-transcriptome sequencing by RNA-Seq for diagnosis of monogenic disorders. *J Invest Dermatol*. 2020;140(6):1117–1126.e1111.
10. Jelin AC, Vora N. Whole exome sequencing: applications in prenatal genetics. *Obstet Gynecol Clin North Am*. 2018;45(1):69–81. doi:10.1016/j.ogc.2017.10.003
11. Klimek L, Förster-Ruhrmann U, Olze H, et al. Empfehlungen zur Überprüfung der Wirksamkeit und Verlaufsdokumentation von Dupilumab bei chronischer Rhinosinusitis mit Nasenpolypen (CRSwNP) im deutschen Gesundheitssystem. *Laryngo-Rhino-Otologie*. 2022;101(11):855–865. doi:10.1055/a-1908-3074
12. Al-Ahmad M, Alsaleh S, Al-Reefy H, et al. Expert opinion on biological treatment of chronic rhinosinusitis with nasal polyps in the Gulf region. *J Asthma Allergy*. 2022;15:1–12. doi:10.2147/JAA.S321017
13. Ohkura N, Sakaguchi S. Transcriptional and epigenetic basis of Treg cell development and function: its genetic anomalies or variations in autoimmune diseases. *Cell Res*. 2020;30(6):465–474. doi:10.1038/s41422-020-0324-7
14. Cardenas A, Fadadu R, Bunyavanich S. Climate change and epigenetic biomarkers in allergic and airway diseases. *J Allergy Clin Immunol*. 2023;152(5):1060–1072. doi:10.1016/j.jaci.2023.09.011
15. Brar T, Marks L, Lal D. Insights into the epigenetics of chronic rhinosinusitis with and without nasal polyps: a systematic review. *Front Allergy*. 2023;4:1165271. doi:10.3389/falgy.2023.1165271
16. Choi H-S, Kim BS, Yoon S, et al. Leukemic Stem Cells and Hematological Malignancies. *Int J Mol Sci*. 2024;25(12):6639. doi:10.3390/ijms25126639
17. Tomasich E, Mühlbacher J, Wöran K, et al. Immune cell distribution and DNA methylation signatures differ between tumor and stroma enriched compartment in pancreatic ductal adenocarcinoma. *Transl Res*. 2024;271:40–51. doi:10.1016/j.trsl.2024.05.005
18. Luong AU, Chua A, Alim BM, Olsson P, Javer A. Allergic fungal rhinosinusitis: the role and expectations of biologics. *J Allergy Clin Immunol Pract*. 2022;10(12):3156–3162. doi:10.1016/j.jaip.2022.08.021
19. Laidlaw TM, Buchheit KM. Biologics in chronic rhinosinusitis with nasal polyposis. *Ann Allergy Asthma Immunol*. 2020;124(4):326–332. doi:10.1016/j.anai.2019.12.001
20. Jiao J, Wang M, Duan S, et al. Transforming growth factor-β1 decreases epithelial tight junction integrity in chronic rhinosinusitis with nasal polyps. *J Allergy Clin Immunol*. 2018;141(3):1160–1163.e9. doi:10.1016/j.jaci.2017.08.045
21. Iwasaki N, Poposki JA, Oka A, et al. Single cell RNA sequencing of human eosinophils from nasal polyps reveals eosinophil heterogeneity in chronic rhinosinusitis tissue. *J Allergy Clin Immunol*. 2024;154(4):952–964. doi:10.1016/j.jaci.2024.05.014
22. Peng Y, Zi -X-X, Tian T-F, et al. Whole-transcriptome sequencing reveals heightened inflammation and defective host defence responses in chronic rhinosinusitis with nasal polyps. *Eur Respir J*. 2019;54(5):1900732. doi:10.1183/13993003.00732-2019
23. Patel GB, Peters AT. The role of biologics in chronic rhinosinusitis with nasal polyps. *Ear Nose Throat J*. 2021;100(1):44–47. doi:10.1177/0145561320964653
24. Ntontsi P, Photiades A, Zervas E, Xanthou G, Samitas K. Genetics and Epigenetics in Asthma. *Int J Mol Sci*. 2021;22(5):2412. doi:10.3390/ijms22052412
25. Yang H, Zou X, Yang S, Zhang A, Li N, Ma Z. Identification of lactylation related model to predict prognostic, tumor infiltrating immunocytes and response of immunotherapy in gastric cancer. *Front Immunol*. 2023;14:1149989.
26. Li H, Li J, Lu T, et al. DZNep attenuates allergic airway inflammation in an ovalbumin-induced murine model. *Mol Immunol*. 2021;131:60–67.
27. Zhu X, Wang X, Wang Y, Zhao Y. Exosomal long non-coding RNA GAS5 suppresses Th1 differentiation and promotes Th2 differentiation via downregulating EZH2 and T-bet in allergic rhinitis. *Mol Immunol*. 2020;118:30–39.
28. Tumes DJ, Onodera A, Suzuki A, et al. The polycomb protein Ezh2 regulates differentiation and plasticity of CD4(+) T helper type 1 and type 2 cells. *Immunity*. 2013;39(5):819–832.
29. Li H, Wen Y, Wu S, et al. Epigenetic modification of enhancer of zeste homolog 2 modulates the activation of dendritic cells in allergen immunotherapy. *Int Arch Allergy Immunol*. 2019;180(2):120–127.
30. Fokkens WJ, Lund VJ, Hopkins C, et al. European Position Paper on Rhinosinusitis and Nasal Polyps 2020. *Rhinology*. 2020;58(Suppl S29):1–464.
31. Love MI, Huber W, Anders S. Moderated estimation of fold change and dispersion for RNA-seq data with DESeq2. *Genome Biol*. 2014;15(12):550.
32. Hou JL, Yang WY, Zhang Q, et al. Integration of metabolomics and transcriptomics to reveal the metabolic characteristics of exercise-improved bone mass. *Nutrients*. 2023;15(7):1694.
33. Larsson C, Andersson KME, Nadali M, Silfverswärd ST, Bokarewa MI, Erlandsson MC. MicroRNA and interleukin 6 interplay in the adipose tissue of rheumatoid arthritis patients. *Clin Exp Rheumatol*. 2023;41(1):32–40.
34. Ito K, Murphy D. Application of ggplot2 to pharmacometric graphics. *CPT Pharmacometrics Syst Pharmacol*. 2013;2(10):e79.
35. Wu T, Hu E, Xu S, et al. clusterProfiler 4.0: a universal enrichment tool for interpreting omics data. *Innovation*. 2021;2(3):100141.
36. Su G, Morris JH, Demchak B, Bader GD. Biological network exploration with Cytoscape 3. *Curr Protoc Bioinformatics*. 2014;47:11–24.
37. Xu J, Liang C, Li J. A signal recognition particle-related joint model of LASSO regression, SVM-RFE and artificial neural network for the diagnosis of systemic sclerosis-associated pulmonary hypertension. *Front Genet*. 2022;13:1078200.
38. Chen B, Khodadoust MS, Liu CL, Newman AM, Alizadeh AA. Profiling Tumor Infiltrating Immune Cells with CIBERSORT. *Methods Mol Biol*. 2018;1711:243–259.
39. Nguyen TV, Vo CT, Vo VM, et al. Phaeanthus vietnamensis ban ameliorates lower airway inflammation in experimental asthmatic mouse model via Nrf2/HO-1 and MAPK signaling pathway. *Antioxidants*. 2023;12(6):1301.
40. Ribeiro CM, Paradiso AM, Carew MA, Shears SB, Boucher RC. Cystic fibrosis airway epithelial Ca2+ i signaling: the mechanism for the larger agonist-mediated Ca2+ i signals in human cystic fibrosis airway epithelia. *J Biol Chem*. 2005;280(11):10202–10209.

41. Müller S, Glaß M, Singh AK, et al. IGF2BP1 promotes SRF-dependent transcription in cancer in a m6A- and miRNA-dependent manner. *Nucleic Acids Res*. 2019;47(1):375–390.
42. Zhang L, Wan Y, Zhang Z, et al. IGF2BP1 overexpression stabilizes PEG10 mRNA in an m6A-dependent manner and promotes endometrial cancer progression. *Theranostics*. 2021;11(3):1100–1114.
43. Verma A, Singh A, Singh MP, et al. EZH2-H3K27me3 mediated KRT14 upregulation promotes TNBC peritoneal metastasis. *Nat Commun*. 2022;13(1):7344.
44. Park SH, Fong KW, Mong E, Martin MC, Schiltz GE, Yu J. Going beyond Polycomb: EZH2 functions in prostate cancer. *Oncogene*. 2021;40 (39):5788–5798.
45. Hanaki S, Shimada M. Targeting EZH2 as cancer therapy. *J Biochem*. 2021;170(1):1–4.
46. Zhou J, Huang S, Wang Z, et al. Targeting EZH2 histone methyltransferase activity alleviates experimental intestinal inflammation. *Nat Commun*. 2019;10(1):2427.
47. Zhang Q, Sun H, Zhuang S, et al. Novel pharmacological inhibition of EZH2 attenuates septic shock by altering innate inflammatory responses to sepsis. *Int Immunopharmacol*. 2019;76:105899.
48. Gao X, Peng Y, Fang Z, et al. Inhibition of EZH2 ameliorates hyperoxaluria-induced kidney injury through the JNK/FoxO3a pathway. *Life Sci*. 2022;291:120258.
49. Mansoori B, Mohammadi A, Ditzel HJ, et al. HMGA2 as a critical regulator in cancer development. *Genes*. 2021;12(2):269.
50. Wang X, Wang J, Wu J. Emerging roles for HMGA2 in colorectal cancer. *Transl Oncol*. 2021;14(1):100894.
51. Li Y, Qiang W, Griffin BB, et al. HMGA2-mediated tumorigenesis through angiogenesis in leiomyoma. *Fertil Steril*. 2020;114(5):1085–1096.
52. Chen Z, Natarajan R. Epigenetic modifications in metabolic memory: what are the memories, and can we erase them? *Am J Physiol Cell Physiol*. 2022;323(2):C570–c582.
53. Li B, Xia Y, Mei S, et al. Histone H3K27 methyltransferase EZH2 regulates apoptotic and inflammatory responses in sepsis-induced AKI. *Theranostics*. 2023;13(6):1860–1875.
54. Ray D, Yung R. Immune senescence, epigenetics and autoimmunity. *Clin Immunol*. 2018;196:59–63.
55. Liao Y, Chen CH, Xiao T, et al. Inhibition of EZH2 transactivation function sensitizes solid tumors to genotoxic stress. *Proc Natl Acad Sci U S A*. 2022;119(3):e2105898119.
56. Deng X, Kong F, Li S, et al. A KLF4/PiHL/EZH2/HMGA2 regulatory axis and its function in promoting oxaliplatin-resistance of colorectal cancer. *Cell Death Dis*. 2021;12(5):485.
57. Lal D, Brar T, Ramkumar SP, et al. Genetics and epigenetics of chronic rhinosinusitis. *J Allergy Clin Immunol*. 2023;151(4):848–868.
58. Shi L, Shi CW, Cheng KW. HMGA2 synergizes with EZH2 to mediate epithelial cell inflammation and apoptosis in septic lung dysfunction. *Ann Clin Lab Sci*. 2022;52(6):938–946.
59. Nakayama T, Lee IT, Le W, et al. Inflammatory molecular endotypes of nasal polyps derived from White and Japanese populations. *J Allergy Clin Immunol*. 2022;149(4):1296–1308.e6.
60. Duan R, Du W, Guo W. EZH2: a novel target for cancer treatment. *J Hematol Oncol*. 2020;13(1):104.
61. Mu S, Wang W, Liu Q, et al. Autoimmune disease: a view of epigenetics and therapeutic targeting. *Front Immunol*. 2024;15:1482728.
62. Straining R, Eighmy W. Tazemetostat: EZH2 Inhibitor. *J Adv Pract Oncol*. 2022;13(2):158–163.
63. Liu Y, Yang Q. The roles of EZH2 in cancer and its inhibitors. *Med Oncol*. 2023;40(6):167.
64. Chen Y, Zhu H, Luo Y, Tong S, Liu Y. EZH2: the roles in targeted therapy and mechanisms of resistance in breast cancer. *Biomed Pharmacother*. 2024;175:116624.
65. Song Y, Liu Y, Li ZM, et al. SHR2554, an EZH2 inhibitor, in relapsed or refractory mature lymphoid neoplasms: a first-in-human, dose-escalation, dose-expansion, and clinical expansion Phase 1 trial. *Lancet Haematol*. 2022;9(7):e493–e503.
66. Li C, Song J, Guo Z, et al. EZH2 inhibitors suppress colorectal cancer by regulating macrophage polarization in the tumor microenvironment. *Front Immunol*. 2022;13:857808.
67. Shahabipour F, Caraglia M, Majeed M, et al. Naturally occurring anti-cancer agents targeting EZH2. *Cancer Lett*. 2017;400:325–335.
68. Serdar CC, Cihan M, Yücel D, et al. Sample size, power and effect size revisited: simplified and practical approaches in pre-clinical, clinical and laboratory studies. *Biochem Med*. 2021;31(1):010502.
69. Kenah E. A potential outcomes approach to selection bias. *Epidemiology*. 2023;34(6):865–872.
70. Lim CY, In J. Randomization in clinical studies. *Korean J Anesthesiol*. 2019;72(3):221–232.